A Comparison of PET Detector Modules Employing Rectangular and Round Photomultiplier Tubes

Simon R. Cherry, Martin P. Tornai, Craig S. Levin, Stefan Siegel, Edward J. Hoffman
Crump Institute for Biological Imaging, Department of Molecular and Medical Pharmacology
UCLA School of Medicine, Los Angeles, CA

Mark S. Andreaco and C.W. Williams
CTI PET Systems Inc., Knoxville, TN

Abstract

We have compared the high resolution BGO detector blocks from the EXACT HR PET system which use two dual-cathode rectangular photomultiplier (PM) tubes with a new block design, the EXACT HR PLUS, which uses four round PM tubes. Despite the lower coupling area between photocathode and scintillator, the HR PLUS block compares favorably with the HR block. The energy resolution averages 20% for the HR PLUS block and 23% for the HR block, with efficiency variations of 17% in both blocks. Additional measurements were carried out on the HR PLUS block to characterize depth of interaction effects and cross-talk between elements. Coincidence line spread function measurements had a FWHM of 3.0 mm in the axial direction and 2.9 mm in the transaxial direction. In light of these results, limitations of the BGO block design are discussed and some solutions proposed.

I. Introduction

The BGO block design [1] has been extremely successful and is now used in the majority of commercial PET systems. The principal performance advantage over single crystal/PM tube configurations is the smaller element size that can be used, which results in high spatial resolution with a good packing fraction. There are also some disadvantages to the block design such as poorer count-rate performance and pile-up [2]. The effects of scatter within the block, and the use of a light sharing scheme to determine the crystal of interaction can result in misidentification of the crystal of interaction [3], resulting in a loss of spatial resolution relative to single crystal/PM tube detectors [4]. Traditionally, the block design has used rectangular cross-section PM tubes which provide close to 100% coupling area between the scintillator block and photocathodes. The cost of these rectangular PM tubes is however quite high and they are not widely available. In contrast, circular cross-section tubes are made by a number of manufacturers and are available at competitive prices. Another benefit of using round PM tubes is that the block naturally assumes square dimensions, leading to uniform axial and transaxial resolution and sampling. This is particularly relevant for 3D PET imaging [5, 6] as it leads to uniform sampling in the projection data. The challenge in using round PM tubes in a PET block detector is to collect sufficient scintillation light from the corner and center crystals, where there is only partial overlap between scintillator and active photocathode regions.

This work was supported by a grant from The Whitaker Foundation and by DOE contract DE-FC03-87ER 60615.

In this study we compare a conventional high resolution BGO block detector which uses rectangular PM tubes (the EXACT HR block) with the new EXACT HR PLUS block which employs four circular PM tubes. We also look in further detail at the performance of the new block design and propose some changes which will be necessary if the resolution potential of the block design is to be fully realized.

II. HR and HR PLUS Blocks: A Comparison

A. Physical Characteristics

The principal characteristics of the EXACT HR and EXACT HR PLUS blocks are summarized in Table I.

Table I: Physical construction of the two detector blocks

	EXACT HR	EXACT HR PLUS
block dim. (mm)	50(A)x23(T)x30(H)	38(A)x36(T)x30(H)
block area (mm^2)	1150	1368
matrix size	8 x 7	8 x 8
area/crystal (mm^2)	20.5	21.4
crystal dim. (mm)	5.9 x 2.9	4.39 x 4.05
PM tubes	2 x dual rectangular	4 x 3/4" round
coupling area (%)	approx. 100	approx. 83

Fig. 1 is a scale drawing of the block geometry with the shaded areas representing the positions of the PM tubes. Although both blocks have similar surface area, the shape of the individual elements are quite different. The coupling area between scintillator and PM tube window is reduced from close to 100% to 80% by the use of round cross-section PM tubes. In both blocks, the depth of the saw cuts varies from approximately 30 mm at the edges to 24 mm at the center.

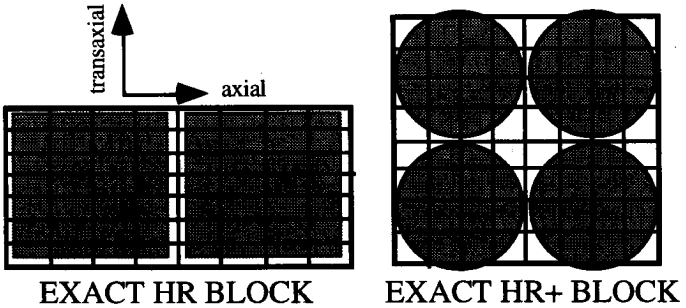

Fig. 1 Scale drawing of HR and HR PLUS detector blocks showing PM tubes superimposed on crystal matrix.

0018-9499/95$4.00

B. Flood Source Measurements

Flood source data was acquired using a F-18 point source, uniformly illuminating the block detector face from a distance of 40-60 cm. With a low threshold set, the outputs from all four PM tubes were amplified (shaping time constant 1 μsec), digitized and stored in list mode for analysis. The trigger pulse for digitization was generated from the sum of the PM tube outputs, fed to a constant fraction discriminator, followed by a gate and delay generator. Fig. 2 shows flood source data for each block, sorted into a position histogram using standard Anger logic [7]. The block was balanced by changing the amplifier outputs until all four quadrants of the block histogram contained a total count density within 1% of each other.

For both blocks, the individual elements are clearly discernible. Boundaries between each element were subsequently determined using a simple minima-tracing algorithm. Notice the slight bowing on the HR histogram caused by the dual cathode PM tubes which share light through their common glass entrance window even for events at the extreme ends of the block.

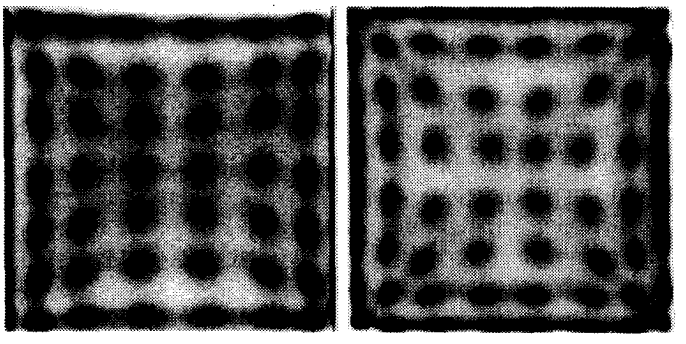

Fig. 2 Flood Source Histogram for HR (left) and HR PLUS (right) detector blocks

Based on the detector boundaries established from the flood source histogram, energy spectra were extracted for each element of the block. Examples from the HR PLUS block are shown in Fig. 3. The centroid of the photopeak was taken to correspond to the pulse height for a 511 keV interaction. The FWHM of the photopeak was then used to compute the energy resolution of each element. Finally, the energy spectrum was integrated between 350 and 650 keV (assuming a linear relation between pulse height and energy) to obtain a measure of the relative efficiencies of the block elements.

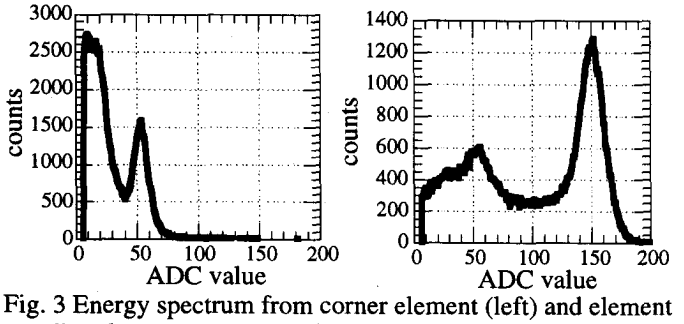

Fig. 3 Energy spectrum from corner element (left) and element directly over photocathode (right) for HR PLUS block.

The energy resolution and relative efficiencies for each element in the blocks are shown in Fig. 4. The distribution of values in these plots reflects the position of the PM tubes relative to the crystal matrix. Areas in which there is poor overlap between detector and photocathode lead to lower pulse height and poorer energy resolution. In the HR PLUS block this is especially apparent at the corners and at the very center of the block.

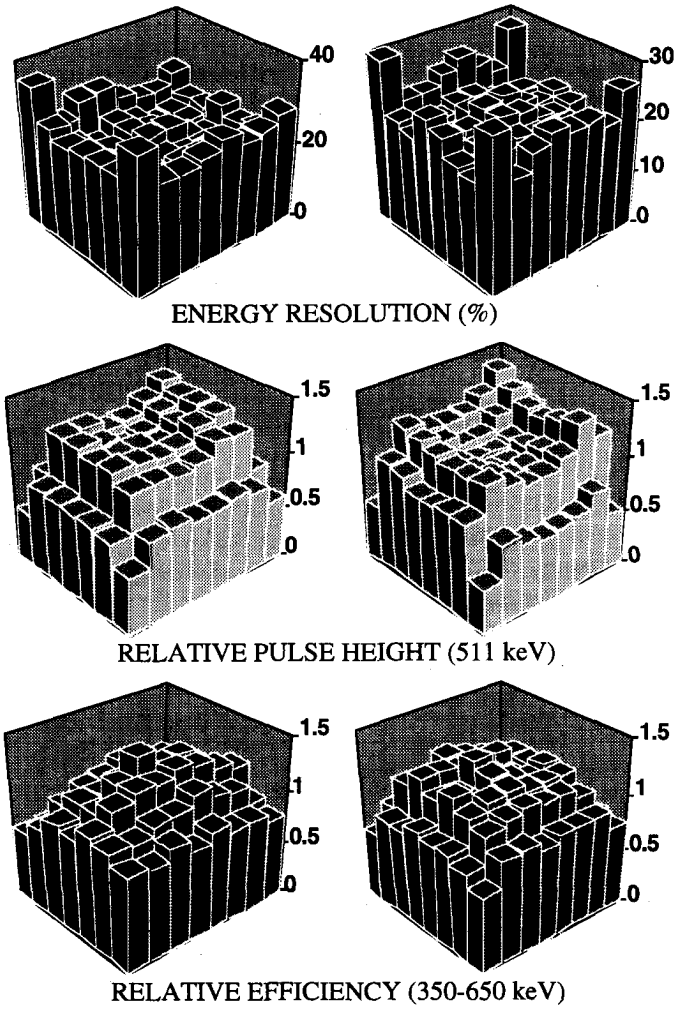

Fig. 4 Plots showing energy resolution, relative pulse height and relative detector efficiency between 350-650 keV for the HR block (left) and the HR PLUS block (right)

The edge and corner detectors of both blocks are actually cut slightly smaller than the other detectors to maintain center-to-center crystal spacing in the tomograph. This reduces the efficiency of these detectors as can be clearly seen in Fig 4. Another factor which tends to increase efficiency at the center of the block relative to the edges is the effect of scatter within the block. Events which deposit all 511 keV of energy but through multiple interactions will be mispositioned with a bias towards the center of the block. A summary of the measurements averaged over all detectors is given in Table II.

Table II: Summary of pulse height, energy resolution and efficiency (350-650 keV) data obtained from flood source irradiation of the two blocks.

	EXACT HR	EXACT HR PLUS
rel. pulse height	s.d./mean = 0.23	s.d./mean = 0.22
energy resolution	23% ± 3.0%	20.3% ± 3.0%
rel. efficiency	s.d./mean = 0.17	s.d./mean = 0.17

C. Point Spread Function Measurements

A Na-22 source (20 μCi, 1 mm diameter), collimated through a 2 mm hole in a 5 cm thick lead brick and in coincidence with a 2 x 2 x 30 mm BGO crystal was used for point spread function (PSF) measurements on the block detectors (Fig. 5).

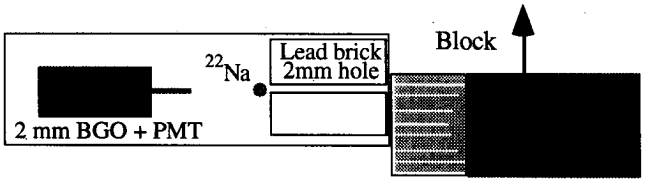

Fig. 5 Set-up used for measuring the PSF in the block.

The block was moved in 0.5 mm steps relative to the source, lead brick and small BGO detector, and data acquired for a central row and column across the block face. The resulting plots (energy window 350-650 keV) are shown in Fig. 6. It is estimated that the spot size on the blocks was around 2 mm.

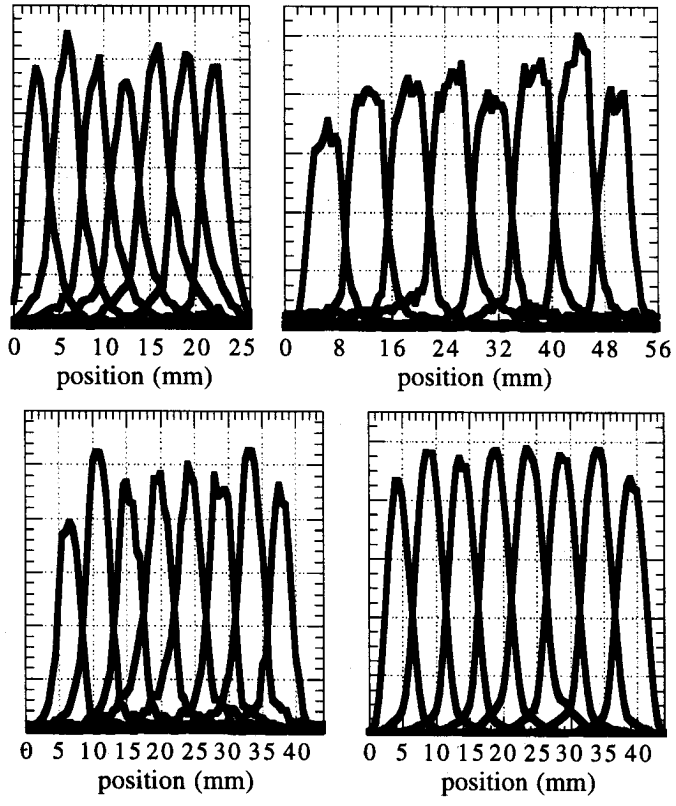

Fig. 6 PSF measurements for the HR (top) and HR PLUS (bottom). Transaxial PSF's are on the left, axial on the right.

The average PSF measurements were 4.1 mm (transaxial) and 4.4 mm (axial) for the HR PLUS block and 3.6 mm (transaxial) and 5.6 mm (axial) for the HR block. These values agree well with the detector dimensions in Table I.

D. Discussion of Comparison Data

The new HR PLUS block has successfully incorporated round PM tubes, while maintaining good performance in the central and corner crystals which only partially overlap active photocathode regions. The HR PLUS block shows slightly improved energy resolution relative to the HR block. This may be a result of higher quantum efficiency in the PM tubes and/or better light collection from square cross-section crystals compared with rectangular cross-section crystals and the slightly higher surface area/length ratio for the HR PLUS detector elements. The element to element variation in pulse height and efficiency are essentially identical for the two blocks, although the characteristic patterns are somewhat different due to the difference in PM tube geometry. Both blocks show PSF measurements which closely reflect the crystal dimensions as expected. Based on these results, we expect the volume resolution of the HR PLUS scanner to be close to that of the HR system, although the distribution between axial and transaxial components is quite different.

Care must be taken when interpreting the absolute values of the results presented. The data is quite sensitive to the electronics used to process the PMT signals, the type of irradiation/collimation used, and in the case of the efficiency measurements, the method used to define the individual detector borders from the block histogram. The values we obtain for the HR agree quite well with measurements taken from a completed HR scanner [8], however we still caution that the absolute values should only be used as a rough guide to predict the performance of blocks in a completed scanner.

III. The HR PLUS Block: Further Expts

A. Depth of Interaction Measurements

We examined the response of the HR PLUS block as a function of the depth of irradiation. The Na-22 source was collimated through a 1.5 mm wide slit between two 5 cm thick lead bricks and data acquired at 4 mm depth intervals. The energy spectra from a range of different depths are shown in Fig. 7 for one inner block element (row 5, column 5). Notice how the pulse height of the photopeak increases as the interaction occurs closer to the photocathode (Fig. 8). In this particular element there is a decrease in light collection at the very deepest position, because here the events occur over a region where there is little overlap with the photocathode. Since the photopeak shifts as a function of depth, the energy resolution at any particular depth is better than the energy resolution measured when the block is irradiated from the front. In this case, the energy resolution at a fixed depth averaged 15% compared to 19% for irradiation over the entire length. The position histograms as a function of depth (not

shown) reveal that there is no significant mispositioning or misidentification of events until you reach the deepest 5-6 mm in the block. This is not surprising given that even the shallowest cut extends 24 mm into the block. Only 5% of the events occur this deep in the block so the effect is negligible.

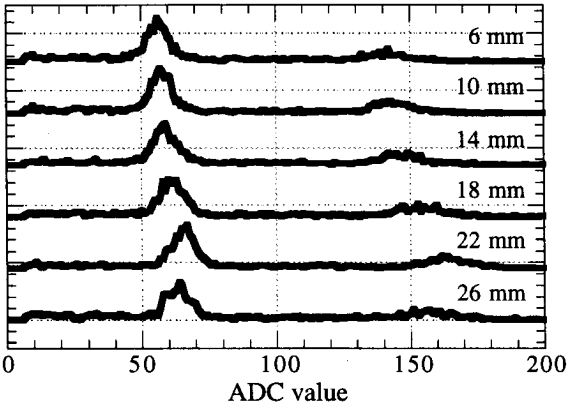

Fig. 7 Energy spectra as a function of depth of interaction. Depth is from front face of block.

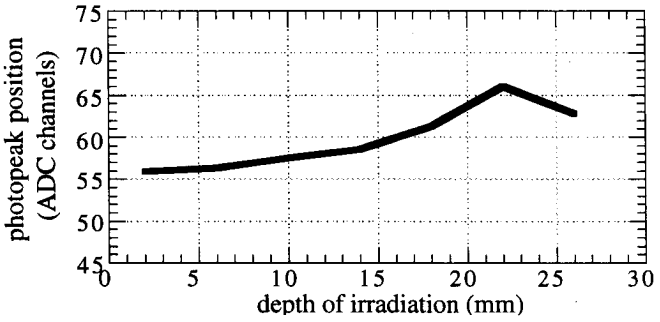

Fig. 8 Photopeak position (511 keV) as a function of depth of interaction for element in row 5, column 5.

B. Detector Identification

The set-up in Fig. 5 was also used to look at the percentage of events which were assigned to the correct detector element. The collimated source was aligned so that it illuminated the center of one of the elements. Based on the detector boundaries, the number of events detected outside of the crystal of interest was examined. Only events in the energy range 350-650 keV were considered. This measurement was repeated for elements across the diagonal of the block. The distribution of the observed events (expressed as a percentage) are shown in Fig. 9. for four different source positions.

There are a number of interesting observations to be made from this data. First, the misidentified events are not confined to the immediately adjacent detectors, but are spread quite uniformly across several detectors. This suggests scatter of the gamma-rays within the block as the major source of mispositioning, rather than errors from the propagation of statistical noise in the determination of the crystal of interaction from the PM tube outputs. This hypothesis is also consistent with the fraction of correctly identified events decreasing as you move towards the middle of the block. Only 45-60% of the events are located in the crystal undergoing irradiation. This is not surprising, given that the probability of a photoelectric interaction at 511 keV in BGO is only 45%. In coincidence, assuming 60% of the events are correctly positioned (the best case), the chance of identifying the correct line of response is only 0.37, thus almost two-thirds of the data will be mispositioned. In a full PET system, scattered gamma rays may be detected by adjacent blocks, making the situation even worse than this. Generally, the mispositioned events are spread across several elements and have the effect of degrading the FWTM rather than the FWHM.

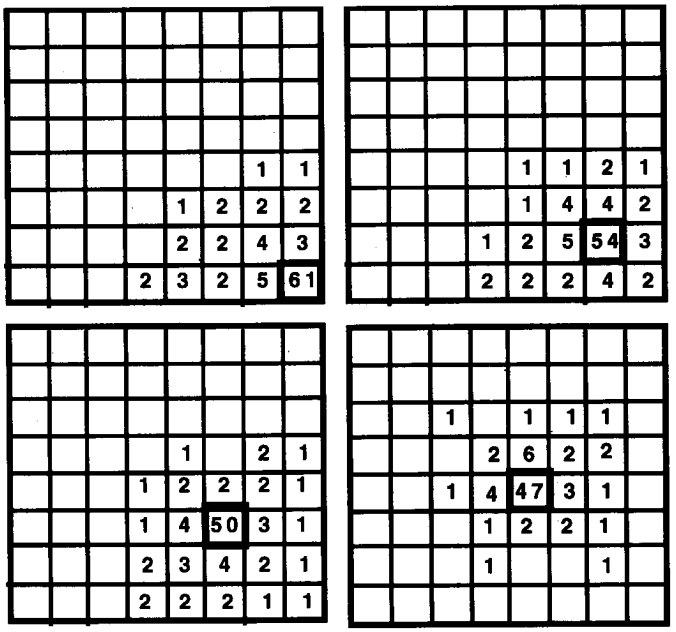

Fig. 9 Distribution of events following irradiation of a single crystal (bold square) for elements along block diagonal.

C. Coincidence Line Spread Function Measurements

Two HR PLUS blocks were placed in coincidence 40 cm apart, and a 20μCi Na-22 source moved in 0.5 mm steps between them. Coincidence data between opposite detector elements was collected as a function of position and the FWHM of the coincidence response measured.

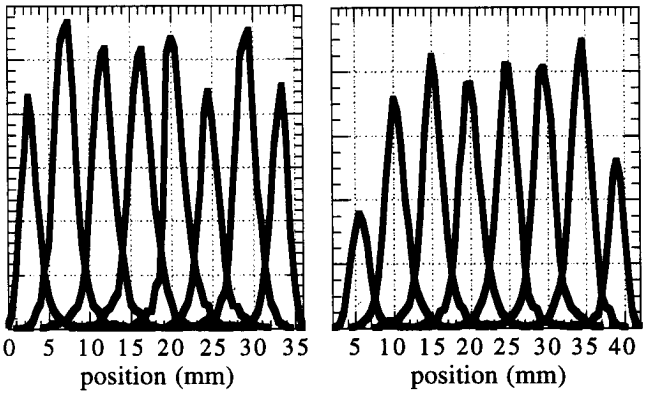

Fig. 10 Coincidence LSF in the transaxial direction (left) and axial direction (right).

Fig. 10 shows the data for a central row (transaxial) and column (axial) across the block. The intrinsic spatial resolution (FWHM) of the block averages 3.0 mm (range 2.4 - 3.4) in the axial direction and 2.9 mm (range 2.4 - 3.5) in the transaxial direction.

IV. DISCUSSION

As observed previously [4], the resolution in block detectors is worse than the geometric D/2 value, because of the effects of block scatter and the statistical variability in position determination, as well as a small contribution from positron range and non-colinearity. In the case of the HR PLUS detectors, the geometric contribution to resolution should be 2.0 mm transaxially and 2.2 mm axially. The measured coincidence LSF averaged 2.9 mm transaxially and 3.0 mm axially. The net effect therefore of these additional factors in the HR PLUS block is to add approximately 2.05 mm in quadrature to the geometric resolution.

The data presented in this paper strongly suggest that scatter within the block, rather than statistical effects due to light sharing, is the predominant source of misidentification in the modern BGO block detector. Given the good separation of detectors seen in the block histogram (Fig. 2), it may seem reasonable to assume that the number of elements in the block detector could be increased without dramatically increasing the fraction of events which are mispositioned. This would lead to higher spatial resolution [9]. There are however several problems with this approach. The coincidence efficiency will decrease due to the additional saw cuts. For example, changing the HR PLUS block from a 8 x 8 to a 12 x 12 matrix would result in an additional 12% loss in coincidence efficiency assuming saw cuts of just 0.25 mm in width. Furthermore, the amount of scintillation light which can be collected also decreases rapidly as the area/length ratio of the elements decreases. More scintillation light can be collected by making the block shorter, but this again has a deleterious effect on efficiency. In addition, one must consider the engineering difficulties of routinely and reliably cutting BGO into such fine arrays.

There are other possibilities for improving block performance, without reducing the element size. Some resolution and contrast improvement can be realized by rejecting or reducing events which scatter in the block, thereby increasing the fraction of events which are correctly located. One approach is to use 'island' boundaries [7, 10] around the elements in the block histogram. As light collection improves, the area of these islands can be made smaller and more block scatter can be rejected. To reject block scatter completely, it will be necessary to return to a single photodetector/crystal configuration. This may be possible in the future using arrays of avalanche or PIN photodiodes on the front surface of the block to determine the crystal of interaction and a single PM tube at the other end for timing [11, 12]. Unfortunately, rejecting all block scattered events would lead to a severe drop in sensitivity and it is not clear that this is a price worth paying for a moderate increase in spatial resolution and image contrast, particularly since the resolution gain is unlikely to be realized in a clinical situation. Further, a large fraction of events scatter in the body, the effect of which would tend to dominate over scatter within the block. Rejecting block scatter might however lead to significant improvements in a high resolution animal PET system, where the sensitivity loss can be compensated for by higher solid angle and far fewer of the events are scattered in leaving the animal.

Finally, it is worth remembering that virtually all human PET studies, even when performed in 3D, are statistics rather than resolution limited. Although the spatial resolution of block detectors can and undoubtedly will continue to improve, it will have little impact on human PET studies unless a significant increase in signal-to-noise is also forthcoming. This may be achieved by improved sensitivity, or by using image reconstruction methods which yield better signal-to-noise in the reconstructed images. Further improvements in resolution are however warranted for animal PET scanners and this may provide the impetus to push PET detector technology forwards in the coming years.

V. REFERENCES

[1] M. E. Casey and R. Nutt, "A multicrystal two dimensional BGO detector system for positron emission tomography," *IEEE Trans Nucl Sci,* vol. NS-33, pp. 460-463, 1986.

[2] G. Germano and E. J. Hoffman, "A study of data loss and mispositioning due to pileup in 2-D detectors in PET," *IEEE Trans Nucl Sci,* vol. NS-37, pp. 671-675, 1990.

[3] M. P. Tornai, E. J. Hoffman, S. R. Cherry, "Effect of refraction index and light sharing on detector element identification for 2D detector modules in positron emission tomography," *Nucl Inst Meth,* vol. A348, pp. 618-622, 1994.

[4] W. W. Moses and S. E. Derenzo, "Empirical observation of resolution degradation in positron emission tomographs utilizing block detectors," *J Nucl Med,* vol. 34, pp. P101, 1993.

[5] S. R. Cherry, M. Dahlbom, E. J. Hoffman, "3D PET using a conventional multislice tomograph without septa," *J Comput Assist Tomogr,* vol. 15, pp. 655-68, 1991.

[6] D. W. Townsend, A. Geissbuhler, M. Defrise, et al., "Fully three-dimensional reconstruction for a PET camera with retractable septa," *IEEE Trans Med Imag,* vol. 10, pp. 505-512, 1991.

[7] M. Dahlbom and E. J. Hoffman, "An evaluation of a two-dimensional array detector for high resolution PET," *IEEE Trans Med Imag,* vol. 7, pp. 264-272, 1988.

[8] K. Wienhard, M. Dahlbom, L. Eriksson, et al., "Performance evaluation of the high resolution PET scanner ECAT EXACT HR," *J Nucl Med,* vol. 34, pp. 101P, 1993.

[9] J. G. Rogers, R. Nutt, M. Andreaco, C. W. Williams, "Testing 144- and 256-crystal BGO block detectors," *IEEE Trans Nucl Sci,* vol. NS-41, pp. 1423-1429, 1994.

[10] P. D. Cutler and E. J. Hoffman, "Use of digital front-end electronics for optimization of a modular PET detector," *IEEE Trans Med Imag,* vol. 13, pp. 408-418, 1994.

[11] W. W. Moses, S. E. Derenzo, R. Nutt, et al., "Performance of a PET detector module utilizing an array of silicon photodiodes to identify the crystal of interaction," *IEEE Trans Nucl Sci,* vol. NS-40, pp. 1036-1040, 1993.

[12] E. Gramsch, M. Szawlowski, S. Zhang, M. Madden, "Fast, high density avalanche photodiode array," *IEEE Trans Nucl Sci,* vol. NS-41, pp. 762-766, 1994.